Constructing Hierarchical Spheres from Large Ultrathin Anatase TiO$_2$ Nanosheets with Nearly 100% Exposed (001) Facets for Fast Reversible Lithium Storage

Jun Song Chen[†], Yi Ling Tan[†], Chang Ming Li[†], Yan Ling Cheah[‡],Deyan Luan[‡], Srinivasan Madhavi[‡], Freddy Yin Chiang Boey[‡], Lynden A. Archer[Ω*], Xiong Wen Lou[†,Ω*]

[†]*School of Chemical and Biomedical Engineering, Nanyang Technological University, 70 Nanyang Drive, Singapore 637457 (Singapore).* [‡] *School of Materials science and Engineering, Nanyang Technological University, 50 Nanyang Avenue, Singapore 639798 (Singapore).* [Ω] *Kaust-Cornell Center for Energy and Sustainability, Cornell University, Ithaca, NY 14853 (U.S.A.)*
Email: xwlou@ntu.edu.sg (X. W. L.); laa25@cornell.edu (L.A.A.)

Abstract: Synthesis of nanocrystals with exposed high-energy facets is a well-known challenge in many fields of science and technology. The higher reactivity of these facets simultaneously makes them desirable catalysts for sluggish chemical reactions and leads to their small populations in an equilibrated crystal. Using anatase TiO$_2$ as an example, we demonstrate a facile approach for creating high surface area, stable nanosheets comprised of nearly 100% exposed (001) facets. Our approach relies on spontaneous assembly of the nanosheets into three-dimensional, hierarchical spheres that stabilizes them from collapse. We show that the high surface density of exposed TiO$_2$ (001) facets leads to fast lithium insertion/deinsertion processes in batteries that mimic features seen in high power electrochemical capacitors.

Introduction

Shape-controlled synthesis of nanocrystals with exposed high-energy/reactive facets is of great importance for both fundamental studies and technological applications (e.g., energy storage in electrochemical capacitors and catalysis) in multiple fields.[1-7] Anatase titanium oxide (TiO_2) with a tetragonal crystal structure is probably the most studied metal oxide.[8-11] The surface energies of its (001) and (101) facets have been calculated to be 0.90 and 0.44 J m^{-2}, respectively.[12] As a result, anatase nanocrystals are usually observed in a truncated bipyramidal shape dominated by energetically stable (101) facets. Although as likely to form during the earliest stages of crystal growth, the more reactive (001) facets are quickly eliminated.[1, 12, 13]

Following the first report of anatase TiO_2 microcrystals with around 47% exposed (001) facets,[14] a series of studies by research groups world-wide have demonstrated synthesis of sheet-like anatase TiO_2 single-crystals with as high as 89% exposed (001) facets.[12, 15-19] However, the construction of hierarchical structures from these interesting anatase TiO_2 nanosheets has not been realized. Another observation is that despite the high percentages of (001) facets that survive crystal growth, the specific surface area of the TiO_2 bearing these facets is unacceptably low, due to the relatively large crystal thickness in the [001] direction. For example, the specific surface area of anatase TiO_2 nanosheets (1.09 μm in width; 260 nm in thickness) with 64% exposed (001) facets is only 1.6 m^2 g^{-1}.[17]

By reducing the thickness in the [001] direction and increasing the two-dimensional lateral size of (001) planes, it should be possible to simultaneously increase the percentage of exposed (001) facets and the specific surface area of sheet-like anatase

TiO$_2$ crystals. Stucky and coworkers have used this approach to synthesize anatase TiO$_2$ nanosheets (NS) with thickness less than 1 nm employing a facile nonaqueous route.[19] Although bounded by the dominant (001) facets, these ultrathin TiO$_2$-NSs are stabilized by large amounts of oleylamine (ca. 43% in weight), and form stacked lamellar structures. Surfactant removal by calcination to obtain pure anatase TiO$_2$ from the ultrathin TiO$_2$-NS lamellar structure is unattractive for at least two reasons: (i) it will likely lead to complete condensation and destruction of the NS; and (ii) it might promote formation of irregular, large anatase TiO$_2$ crystals, which defeat the very purpose of the oleylamine stabilizing layer. One way to obtain thermally stable ultrathin NSs is to grow them into a three-dimensionally self-organized architecture as nicely demonstrated for ultrathin zeolite NSs most recently.[20]

Herein, we report a simple synthesis of hierarchical spheres self-organized from ultrathin anatase TiO$_2$ nanosheets (NS) with nearly 100% exposed (001) facets. Several earlier studies have demonstrated that the highly-reactive (001) facets of anatase TiO$_2$-NS exhibit superior photocatalytic activities when normalized by the surface area.[12, 15, 16] Here we show that these facets also provide unusual opportunities for electrochemical energy storage. In this particular application we take advantage of both the high surface activity of the synthesized anatase TiO$_2$-NS hierarchical spheres (TiO$_2$-NSHS) and the excellent "bulk" properties imparted by their geometry. Specifically, the extremely short transport length-scales in the [001] direction and a well-defined nanoporous structure facilitate fast, reversible lithium insertion/extraction, a requirement for high-power lithium-ion batteries.[21, 22]

Materials Synthesis. In a typical synthesis, 0.03 ml of diethylenetriamine (DETA; 99%, Sigma-Aldrich) was added into 42 ml of isoproponal (IPA). After the solution was gently stirred for a few minutes, 1.5 ml of titanium (IV) isopropoxide (TIP; 97%, Sigma-Aldrich) was added. The reaction solution was then transferred into a 60 ml Teflon-lined stainless steel autoclave and kept in an electric oven at 200 ^{o}C for 24 h. It should be noted that any disturbance during the reaction, e.g., opening of oven door, need to be avoided to assure the successful formation of the desired structure. The autoclave was then taken out from the oven and left to cool down naturally to room temperature. The white precipitate was harvested via centrifugation and washed thoroughly with ethanol before drying at 60 ^{o}C overnight. All products are calcined at 400 ^{o}C for 2 h with a heating rate of 1 ^{o}C min^{-1} to obtain highly crystalline anatase phase.

Materials Characterizations. The morphology of products was examined by transmission electron microscope (TEM; JEOL, JEM-2100F, 200 kV), field-emission scanning electron miscroscope (FESEM; JEOL, JSM-6700F, 5 kV). The elemental compositions of the samples were analyzed with energy-dispersive X-ray spectroscopy (EDX) attached to FESEM. Crystallographic information of the samples was investigated with X-ray powder diffraction (XRD; Bruker, D8 - Advance X-Ray Diffractometer, Cu Kα, λ = 1.5406 Å). The surface area of the sample was measured using Quantachrome Instruments, Autosorb AS-6B. For the uncalcined sample, the thermogravimetric analysis (TGA) was carried out in a flow of air with a temperature ramp of 5 ^{o}C min^{-1}.

Electrochemical Measurements. The electrochemical measurements were carried out using two-electrode Swagelok cells with pure lithium metal as the counter and also the

reference electrodes at room temperature. The working electrode consists of active material (e.g., TiO_2-NS spheres), a conductive agent (carbon black, Super-P-Li), and a polymer binder (polyvinylidene difluoride, PVDF, Aldrich) in a weight ratio of 70:20:10. The electrolyte used was 1.0 M $LiPF_6$ in a 50:50 (w/w) mixture of ethylene carbonate and diethyl carbonate. Cell assembly was carried out in an Ar-filled glovebox with concentrations of moisture and oxygen below 1.0 ppm. Cyclic voltammetry (CV, 1 V – 3 V, 0.2 mV/s) was performed using an electrochemical workstation (CHI 660C). The charge/discharge tests were performed using a NEWARE battery tester at different current rates (1 C = 170 mA g^{-1}) with a voltage window of 1 V – 3 V.

Results and Discussions

Our anatase TiO_2-NSHSs are obtained by calcining the solvothermally synthesized amine-stabilized TiO_2-NSHS (Figure 1A) at 400 ^{o}C in static air (see the experimental section). The high crystallinity and phase purity of the resultant material are confirmed by X-ray diffraction (XRD, Figure 1B). All the identified peaks (pattern II in Figure 1B) can be perfectly indexed to anatase TiO_2 (JCPDS card no. 21-1272, S.G.: $I4_1/amd$, a_o = 3.7852 Å, c_o = 9.5139 Å). The pristine uncalcined TiO_2-NSHS is poorly crystalline in anatase phase (pattern I in Figure 1B), where the two weak peaks located at 2θ of 25° and 48° can be attributed to anatase (101) and (200) diffractions, respectively. Thermogravimetric analysis (TGA, Figure 2) and CHN elemental analysis reveal that it contains approximately 21 wt% of organic species, while the weight loss of about 12 wt% below 100 ^{o}C in Figure 2 could be attributed to the evaporation of adsorbed moisture or gaseous contents in this highly porous material (discussed shortly).

5

The morphology of the as-obtained anatase TiO_2-NSHSs is characterized by scanning electron microscopy (SEM) and transmission electron microscopy (TEM) as shown in Figure 3. It is immediately apparent that the spheres are quite uniform, with an average size of ~1 μm (Figure 3 A and C). From the high–magnification micrographs (Figure 3 B and D), the constituent NSs are easily visible, and seen to adopt random orientations. The gradual contrast of the TEM image (Figure 3D) from the edge to the center of the sphere indicates that the entire sphere is indeed composed of self-organized TiO_2-NSs. Phase purity and chemical composition of the product are confirmed by energy-dispersive X-ray spectroscopy (EDX, Figure 3E) analysis, which shows strong Ti and O signals. The self-assembly of TiO_2-NSs renders a nanoporous structure as confirmed by the N_2 adsorption/desorption isotherm shown in Figure 3F. It gives a type IV isotherm with a type H3 hysteresis loop indicating a mesoporous structure.[23] The relatively narrow pore size distributions (Figure 3F, inset) calculated by the Barrett-Joyner-Halenda (BJH) method from both branches of the isotherm signify that most of the pores are in the range of 5 – 15 nm in size. Such a porous structure gives rise to a very high specific surface area of 170 $m^2 g^{-1}$, calculated by the Brunauer-Emett-Teller (BET) method.

High resolution (HR) TEM analysis is employed to determine the crystal facets. Figure 4A shows part of a single nanosheet with visible lattice fringes. It can be observed that two sets of lattices are present and that they are oriented perpendicular to each other with an equal inter-fringe spacing of 0.19 nm, corresponding to anatase (020) and (200) planes. The fast-Fourier-transform (FFT) pattern (Fig. 4A, inset) of the same region can be indexed to diffraction spots of the [001] zone.[14] Therefore it can be concluded that the TiO_2-NS is bounded by (001) facets on both the top and bottom. Figure 4C displays the

HRTEM image taken from region 1 (marked by a dotted circle) in Figure 4B. The distance of the visible lattice fringes over a large area is measured to be 0.19 nm, indicating that the TiO_2-NSs are single crystals when lying flat. The dark line in the TEM image (Figure 4B, region 2) demarcates the edge of a curved NS that is approximately perpendicular to the support film. The corresponding HRTEM image (Figure 4D) also reveals lattice fringes with a distance of 0.19 nm, which is again precisely the inter-plane spacing of (020) or (200) of anatase. These dark lines can be used to estimate the thickness of the NS to be only 3 nm, which explains its curved feature and high specific surface area of 170 m^2 g^{-1}. Assuming that each TiO_2-NS is as long as it is wide, a sheet thickness of ~ 3 nm and size of 100 – 300 nm implies that 95 – 99 % of the exposed surfaces are (001) facets.

To understand the mechanism of forming such a nanosheet-based hierarchical structure, different experimental conditions were investigated. Generally, no nanosheet structures were formed using amines with other chain lengths, e.g., methylamine, ethylenediamine, oleylamine, or 1-hexadecylamine, indicating that DETA is particularly suitable and effective to produce nanosheet-like structures in the current solvothermal synthetic system. Moreover, the stabilizing effect of DETA can be further revealed by increasing its relative concentration in the reaction medium. When the amount of TIP is decreased to 0.6 ml, chain-like structures assembled from ultrathin TiO_2 NSs are formed (Figure 5), where the organization of the NSs is much lesser compact. It can then be hypothesized that, the emerging (001) high energy surfaces will be effectively stabilized by DETA in the solvothermal system, which prohibits their growth long the [001] direction. After prolonged reaction, due to the 2-dimensional lateral growth of such facets, they will

develop into large ultrathin NSs. Because of their ultrathin feature, these NSs are highly flexible and can thus readily self-organize into different hierarchical architectures while still maintaining the maximized exposure of (001) facets.

Anatase TiO_2 has been intensively studied both experimentally and theoretically as the host structure for reversible lithium insertion/extraction.[24-33] The principal reaction that governs the electrochemical processes in a TiO_2/Li half-cell is thought to be: $TiO_2 + xLi^+ + xe^- \rightarrow Li_xTiO_2$ (1), with the maximum insertion coefficient x determined to be about 0.5.[34-37] This leads to a theoretical charge storage capacity of 167.5 mA h g^{-1}.[28] It is known that the diffusion of Li^+ ions in the anatase framework occurs along a reaction path connecting the vacant octahedral interstitial sites,[25, 26, 29] which makes diffusion along the c-axis (i.e., the [001] direction) more efficient compared to in the ab-plane. The preponderance of accessible (001) facets in our TiO_2-NSHSs presages unusual (fast) lithium insertion/extraction kinetics.

Figure 6A displays representative cyclic voltammograms (CV) of the anatase TiO_2-NSHS. In agreement with previous studies, two well-defined current peaks are observed at 1.55 V (cathodic sweep) and 2.2 V (anodic sweep). The peak at 1.55 V corresponds to the biphasic transition from tetragonal anatase ($I4_1/amd$) to orthorhombic $Li_{0.5}TiO_2$ (*Imma*) when the insertion coefficient x in reaction (1) reaches about 0.05.[25, 26, 28] Interestingly, it can be observed that the intensity of both peaks increases during the subsequent scans, suggesting a possible activating process in the electrode material.[38] More strikingly, there is no apparent irreversible process observed in the first cathodic scan indicating a high Coulombic efficiency for lithium extraction. This observation is quite unusual for anatase TiO_2.

Figure 6B depicts the charge-discharge voltage profiles of the TiO_2-NSHS electrode for the first few cycles at a current rate of 5 C (850 mA g^{-1}). The result is generally consistent with the above CV analysis as well as previously reported data,[30, 39] where two voltage plateaus appear at about 1.7 V and 2.1 V during the discharge and charge processes, respectively. The discharge curves clearly show that the lithium insertion process can be divided into three different stages.[39] The first stage is represented by the sharp drop of the potential from the open circuit voltage to a value around 1.7 V, which is just before onset of the plateau region. The next stage is the process of lithium insertion into the vacancy sites of the TiO_2 crystal structure, corresponding to the short horizontal plateau region. The final stage is the gradual decay of the voltage after the plateau region, reflecting that the lithium ions are further inserted into the surface layer of the electrode material.[39] The insertion process gives a first discharge capacity of 204 mA h g^{-1}, and a subsequent charge capacity of 169 mA h g^{-1}, leading to an irreversible capacity loss of only 17%. This should be considered very low when compared to other anatase TiO_2 electrodes, as the initial irreversible capacity loss reported is generally in the range of 30 – 40%.[28, 40-42] In the second cycle, the discharge capacity decreases to 175 mA h g^{-1} with a corresponding charge capacity of 165 mA h g^{-1}, leading to a much higher Coulumbic efficiency of 94%. This value further increases to 97% in the fifth charge-discharge cycle, indicating that the irreversible capacity loss due to trapping of Li^+ inside TiO_2 framework decreases rapidly upon cycling.[30]

Figure 6C displays the high reversibility of the underlying electrochemical reactions over many charge/discharge cycles, at different current densities (C-rates). When charged at a rate of 1C, a lithium ion battery requires about 1 hour to approach its full charge

capacity. Remarkably, at a rate of 1C (170 mA g^{-1}) a reversible capacity of 174 mA h g^{-1} can be retained after more than 100 charge-discharge cycles. This corresponds to a lithium insertion coefficient of 0.52, which is slightly higher than the previously determined maximum value of 0.5. This difference is not unusual for high-surface area nanostructures and is here attributed to the presence of an abundance of active surface sites for lithium storage.[43] As usual, the reversible capacity decreases to 136 mA h g^{-1} after 100 cycles when the C-rate is increased to 5 C (850 mA g^{-1}). Further increasing the C-rate to 10 C (1700 mA g^{-1}) leads to small decrease in capacity, nicely confirming that the short diffusion path length in our ultrathin TiO$_2$ nanosheets leads to highly efficient solid state diffusion of Li$^+$ ions. These high-rate capacities are probably among the best reported values for any TiO$_2$-based electrodes tested under similar conditions.

To investigate the rate capability, our TiO$_2$-NSHS is discharged and charged at various current rates, with the results shown in Figure 7A. It can be clearly observed that our TiO$_2$-NSHS shows excellent capacity retention at different rates. Even at a high current rate of 20 C (3400 mA g^{-1}), a reversible capacity of 95 mA h g^{-1} can still be delivered, demonstrating a magnificent high rate performance. Moreover, a capacity of 169 mA h g^{-1} can be resumed when the rate is reduced back to 1 C. Figure 7B illustrates the current rate dependence of the discharge capacities of the TiO$_2$-NSHS. Apparently, the capacities drop with increasing current densities (equivalent to power density when multiply by the average discharge voltage). At current rates of 0.5 C (85 mA g^{-1}), 1 C, and 5 C, specific capacities of 224 mA h g^{-1}, 192 mA h g^{-1}, and 170 mA h g^{-1} can be obtained, respectively. It is important to mention that, the first discharge capacity of 300 mA h g^{-1} can be reached at the current rate of 0.5 C, corresponding to a lithium insertion coefficient of

0.88, which is significantly higher than the theoretical value of 0.5. This first-cycle high discharge capacity is generally attributed to surface phenomena such as the irreversible decomposition of electrolyte accompanying the formation of solid electrolyte interface (SEI),[39, 43, 44] as well as the ultrathin nanosheets granting efficient transport of lithium ions.[30] When a current as high as 10 C (1700 mA g^{-1}) is used, our TiO$_2$-NSHS is still able to deliver a reversible capacity of 150 mA h g^{-1}.

In order to further understand the enhanced lithium storage properties of these anatase TiO$_2$-NSHS, we have carried out post-mortem studies after 100 charge-discharge cycles at 5 C (850 mA g^{-1}). As shown in Figure 8 A and B, the overall spherical structures can be fairly retained although the detailed nanosheet structures become somehow diminished. This is understandable as these nanosheets might be too thin but large to withstand the high-rate insertion/extraction of lithium ions over extended cycling. Nevertheless, the nanosheet structure might still exist in the resulting fine particles. Our recent study shows that the nanosheet structure can be completely retained for smaller but thinker (about 10 nm) free-standing anatase TiO$_2$ nanosheets.[38] Surprisingly, the XRD analysis suggests that the anatase crystal structure can also be sustained (Figure 7C), as there is no noticeable change in the intensities of the dominant (101) peaks before and after the electrochemical test. This observation is a good demonstration of the bulk structural stability of our TiO$_2$-NSHS, considering that the long-range crystal ordering of the electrode material is usually lost after extended galvanostatic cycling.[45]

11

Conclusions

In summary, a simple approach is presented for synthesizing uniform hierarchical spheres self-assembled from ultrathin anatase TiO_2 nanosheets (~ 3 nm in thickness and a few hundred nm in lateral size) with nearly 100% exposed (001) facets. These hierarchical spheres manifest a 3D nanoporous structure with a high specific surface area of about 170 m^2 g^{-1}. Inspired by the unique structure and inherently short transport path length of the assembled TiO_2 nanosheets, we evaluate their ability to reversibly insert/release lithium for high power density electrochemical energy storage in batteries. Our results show that anatase TiO_2-NS spheres manifest unusually high Coulombic efficiency for lithium extraction, excellent capacity retention, and superior rate behavior. In addition to their promise for high-power lithium-ion battery electrodes, we anticipate that anatase TiO_2 nanosheet assemblies will provide long sought after materials solutions in multiple fields, including photocatalysis and dye-sensitized solar cells.

**References**

(1)   Yin, Y.; Alivisatos, A. P. *Nature* **2005,** *437*, 664.

(2)   Lim, B.; Jiang, M. J.; Camargo, P. H. C.; Cho, E. C.; Tao, J.; Lu, X. M.; Zhu, Y. M.; Xia, Y. N. *Science* **2009,** *324*, 1302.

(3)   Tian, N.; Zhou, Z. Y.; Sun, S. G.; Ding, Y.; Wang, Z. L. *Science* **2007,** *316*, 732.

(4)   Schrinner, M.; Ballauff, M.; Talmon, Y.; Kauffmann, Y.; Thun, J.; Moller, M.; Breu, J. *Science* **2009,** *323*, 617.

(5)   Hu, L. H.; Peng, Q.; Li, Y. D. *J. Am. Chem. Soc.* **2008,** *130*, 16136.

(6)   Lee, H.; Habas, S. E.; Kweskin, S.; Butcher, D.; Somorjai, G. A.; Yang, P. D. *Angew. Chem. Int. Ed.* **2006,** *45*, 7824.

(7)   Zhu, J.; Wang, S. H.; Bian, Z. F.; Cai, C. L.; Li, H. X. *Res. Chem. Intermed.* **2009,** *35*, 769.

(8)   Gratzel, M. *Nature* **2001,** *414*, 338.

(9)   Schloegl, R. *Nat. Mater.* **2008,** *7*, 772.

(10)   Yang, H. G.; Zeng, H. C. *Angew. Chem. Int. Ed.* **2004,** *43*, 5206.

(11)   Wang, D. H.; Liu, J.; Huo, Q. S.; Nie, Z. M.; Lu, W. G.; Williford, R. E.; Jiang, Y. B. *J. Am. Chem. Soc.* **2006,** *128*, 13670.

(12)   Zhang, D. Q.; Li, G. S.; Yang, X. F.; Yu, J. C. *Chem. Comm.* **2009**, 4381.

(13)   Penn, R. L.; Banfield, J. F. *Geochim. Cosmichim. Acta* **1999,** *63*, 1549.

(14)   Yang, H. G.; Sun, C. H.; Qiao, S. Z.; Zou, J.; Liu, G.; Smith, S. C.; Cheng, H. M.; Lu, G. Q. *Nature* **2008,** *453*, 638.

(15)   Han, X.; Kuang, Q.; Jin, M.; Xie, Z.; Zheng, L. *J. Am. Chem. Soc.* **2009,** *131*, 3152.

(16)   Liu, G.; Yang, H. G.; Wang, X.; Cheng, L.; Pan, J.; Lu, G. Q.; Cheng, H.-M. *J. Am. Chem. Soc.* **2009,** *131*, 12868.

(17)   Yang, H. G.; Liu, G.; Qiao, S. Z.; Sun, C. H.; Jin, Y. G.; Smith, S. C.; Zou, J.; Cheng, H. M.; Lu, G. Q. *J. Am. Chem. Soc.* **2009,** *131*, 4078.

(18)   Dai, Y. Q.; Cobley, C. M.; Zeng, J.; Sun, Y. M.; Xia, Y. N. *Nano Lett.* **2009,** *9*, 2455.

(19)   Wu, B. H.; Guo, C. Y.; Zheng, N. F.; Xie, Z. X.; Stucky, G. D. *J. Am. Chem. Soc.* **2008,** *130*, 17563.

(20)   Choi, M.; Na, K.; Kim, J.; Sakamoto, Y.; Terasaki, O.; Ryoo, R. *Nature* **2009,** *461*, 246.

(21)   Arico, A. S.; Bruce, P.; Scrosati, B.; Tarascon, J. M.; Van Schalkwijk, W. *Nat. Mater.* **2005,** *4*, 366.

(22)   Kang, B.; Ceder, G. *Nature* **2009,** *458*, 190.

(23)   Kruk, M.; Jaroniec, M. *Chem. Mater.* **2001,** *13*, 3169.

(24)   Armstrong, A. R.; Armstrong, G.; Canales, J.; Garcia, R.; Bruce, P. G. *Adv. Mater.* **2005,** *17*, 862.

(25)   Lunell, S.; Stashans, A.; Ojamae, L.; Lindstrom, H.; Hagfeldt, A. *J. Am. Chem. Soc.* **1997,** *119*, 7374.

(26)   Wagemaker, M.; Kentgens, A. P. M.; Mulder, F. M. *Nature* **2002,** *418*, 397.

(27)   Armstrong, G.; Armstrong, A. R.; Bruce, P. G.; Reale, P.; Scrosati, B. *Adv. Mater.* **2006,** *18*, 2597.

(28)   Lou, X. W.; Archer, L. A. *Adv. Mater.* **2008,** *20*, 1853.

(29)   Deng, D.; Kim, M. G.; Lee, J. Y.; Cho, J. *Energy Environ. Sci.* **2009,** *2*, 818.

(30)   Das, S. K.; Darmakolla, S.; Bhattacharyya, A. J. *J. Mater. Chem.* **2010,** *20*, 1600.

(31)   Ortiz, G. F.; Hanzu, I.; Djenizian, T.; Lavela, P.; Tirado, J. L.; Knauth, P. *Chem. Mater.* **2009,** *21*, 63.

(32)   Cheah, S. K.; Perre, E.; Rooth, M.; Fondell, M.; Harsta, A.; Nyholm, L.; Boman, M.; Gustafsson, T.; Lu, J.; Simon, P.; Edstrom, K. *Nano Lett.* **2009,** *9*, 3230.

(33)   Kavan, L.; Kalbac, M.; Zukalova, M.; Exnar, I.; Lorenzen, V.; Nesper, R.; Graetzel, M. *Chem. Mater.* **2004,** *16*, 477.

(34)   Cava, R. J.; Murphy, D. W.; Zahurak, S.; Santoro, A.; Roth, R. S. *J. Solid State Chem.* **1984,** *53*, 64.

(35)   Ohzuku, T.; Kodama, T.; Hirai, T. *J. Power Sources* **1985,** *14*, 153.

(36)   Kavan, L.; Gratzel, M.; Rathousky, J.; Zukal, A. *J. Electrochem. Soc.* **1996,** *143*, 394.

(37)   Lindstrom, H.; Sodergren, S.; Solbrand, A.; Rensmo, H.; Hjelm, J.; Hagfeldt, A.; Lindquist, S. E. *J. Phys. Chem. B* **1997,** *101*, 7717.

(38)   Chen, J. S.; Lou, X. W. *Electrochem. Comm.* **2009,** *11*, 2332.

(39)   Jiang, C. H.; Wei, M. D.; Qi, Z. M.; Kudo, T.; Honma, I.; Zhou, H. S. *J. Power Sources* **2007,** *166*, 239.

(40)   Gao, X. P.; Lan, Y.; Zhu, H. Y.; Liu, J. W.; Ge, Y. P.; Wu, F.; Song, D. Y. *Electrochem. Solid-state Lett.* **2005,** *8*, A26.

(41)   Xu, J.; Jia, C.; Cao, B.; Zhang, W. F. *Electrochem. Acta* **2007,** *52*, 8044.

(42)   Song, B.; Liu, S. W.; Jian, J. K.; Lei, M.; Wang, X. J.; Li, H.; Yu, J. G.; Chen, X. L. *J. Power Sources* **2008,** *180*, 869.

(43)   Guo, Y. G.; Hu, Y. S.; Maier, J. *Chem. Comm.* **2006**, 2783.

(44)   Sudant, G.; Baudrin, E.; Larcher, D.; Tarascon, J. M. *J. Mater. Chem.* **2005,** *15*, 1263.

(45)   Chen, J. S.; Lou, X. W. *J. Power Sources* **2010,** *195*, 2905.

Figures and Captions
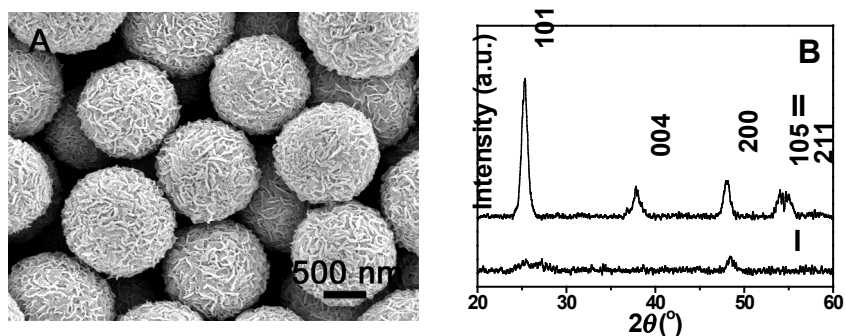
Figure 1. (A) Field-emission scanning electron microscopy (FESEM) image of the as-synthesized TiO$_2$-NS spheres. (B) X-ray diffraction (XRD) patterns of the TiO$_2$-NS spheres: (I) as synthesized, and (II) after calcination at 400 ^{o}C.
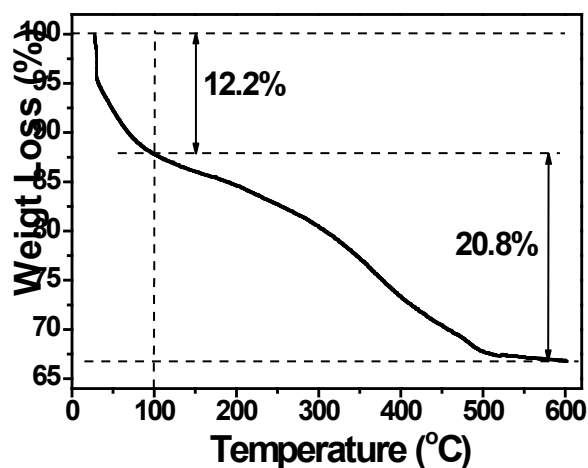

Figure 2. Thermogravimetric analysis (TGA) curve of the as-synthesized TiO$_2$-NS spheres in an air flow at a temperature ramp of 5 ^{o}C min^{-1}.
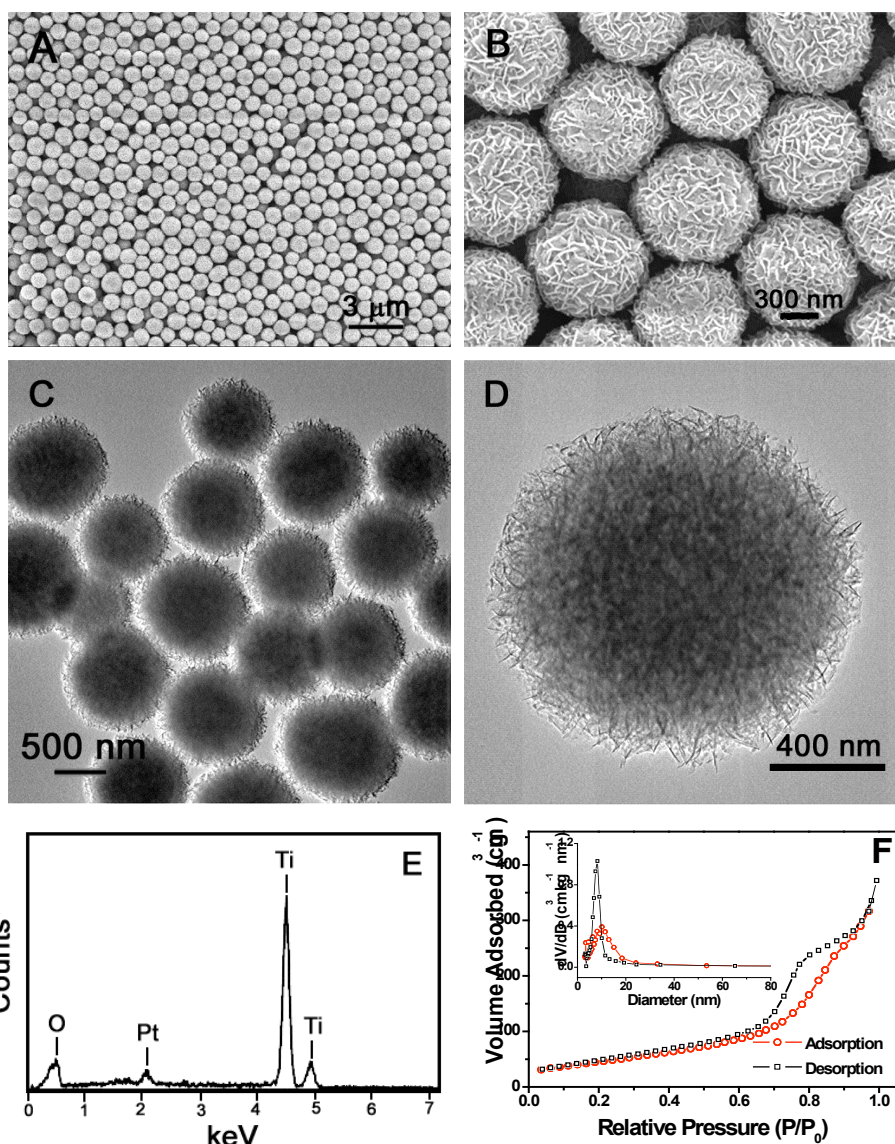
Figure 3. FESEM images (A and B) and transmission electron microscopy (TEM) images (C and D) of as-prepared anatase TiO_2-NS spheres. (E) Energy-dispersive X-ray spectroscopy (EDX) analysis of the anatase TiO_2-NS spheres. The Pt signal arises from the Pt coating during sample preparation. (F) N_2 adsorption/desorption isotherm of the as-prepared anatase TiO_2-NS spheres. The inset shows the pore size distributions calculated by the Barrett-Joyner-Halenda (BJH) method.
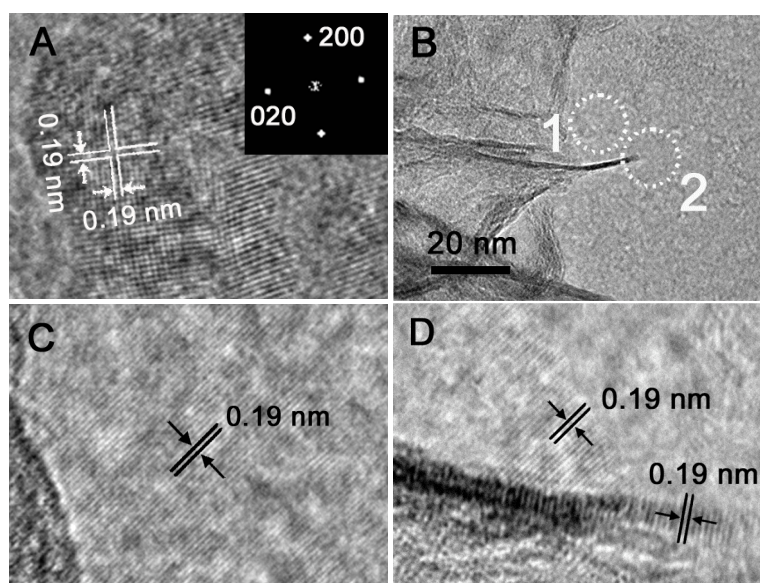
**Figure 4.** (A) HRTEM image of an ultrathin TiO$_2$-NS showing two sets of perpendicular lattice fringes with a spacing of 0.19 nm. The inset shows the FFT pattern indexed to the [001] zone. (B) TEM image recorded around the edge of a TiO$_2$-NS sphere. (C) and (D) HRTEM images of regions 1 and 2 marked with white dotted circles in (B), respectively. Both images show lattice fringes with a spacing of 0.19 nm.
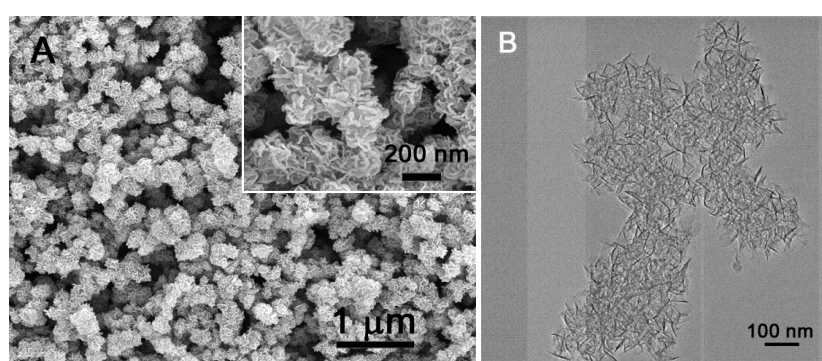

Figure 5. FESEM (A) and TEM (B) images of the chain-like structure assembled from ultra-thin TiO$_2$-NSs when 0.6 ml of TIP is used in the synthesis. The inset in (A) shows a FESEM image at a higher magnification.
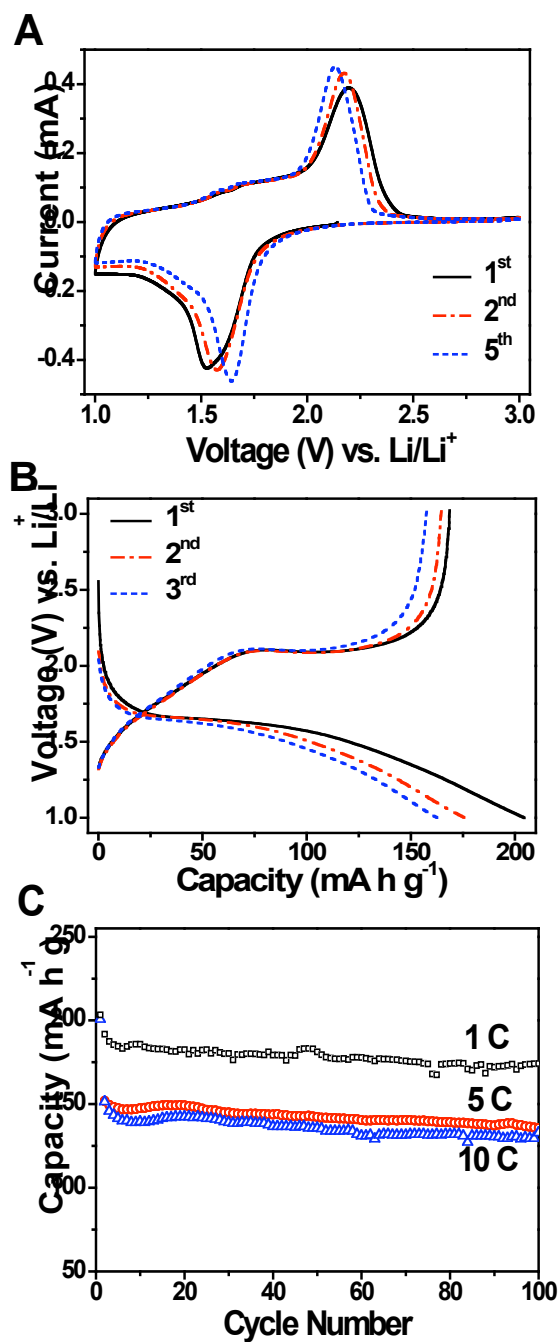
Figure 6. (A) Representative CVs at a scan rate of 0.2 mV s^{-1} for the 1st, 2nd, and 5th cycles. (B) charge-discharge profiles at a current rate of 5 C (850 mA g^{-1}) for the 1st, 2nd, and 5th cycles. (C) Cycling performance at different C-rates. All measurements were conducted with a voltage window of 1.0 – 3.0 V.

A

B
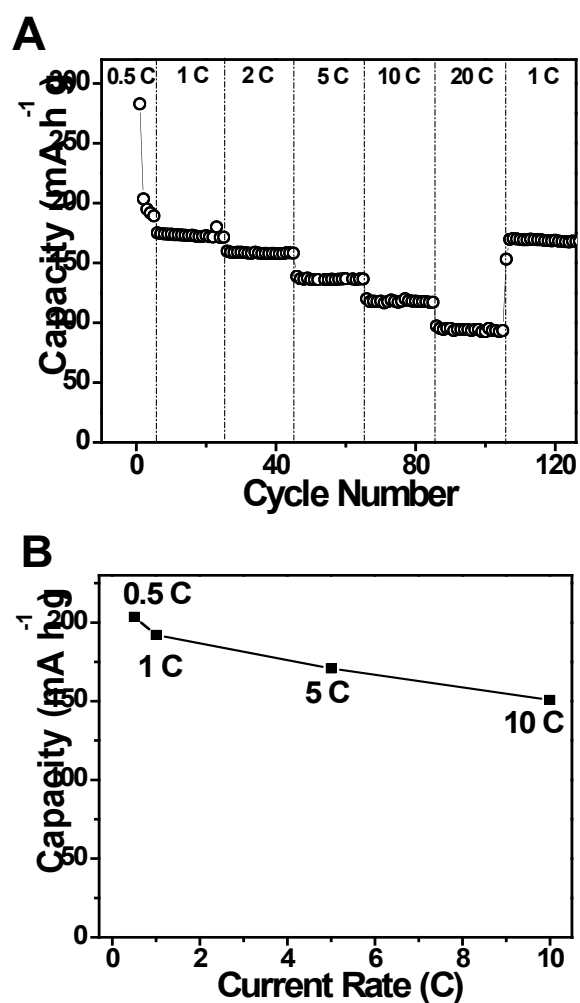
Figure 7. (A) Cycling performance of the anatase TiO$_2$-NSHS at various charge-discharge rates. (B) The current rate dependence of the discharge capacities of the anatase TiO$_2$-NSHS. The capacities are extracted from the second cycle. All measurements were conducted with a voltage window of 1.0 – 3.0 V.
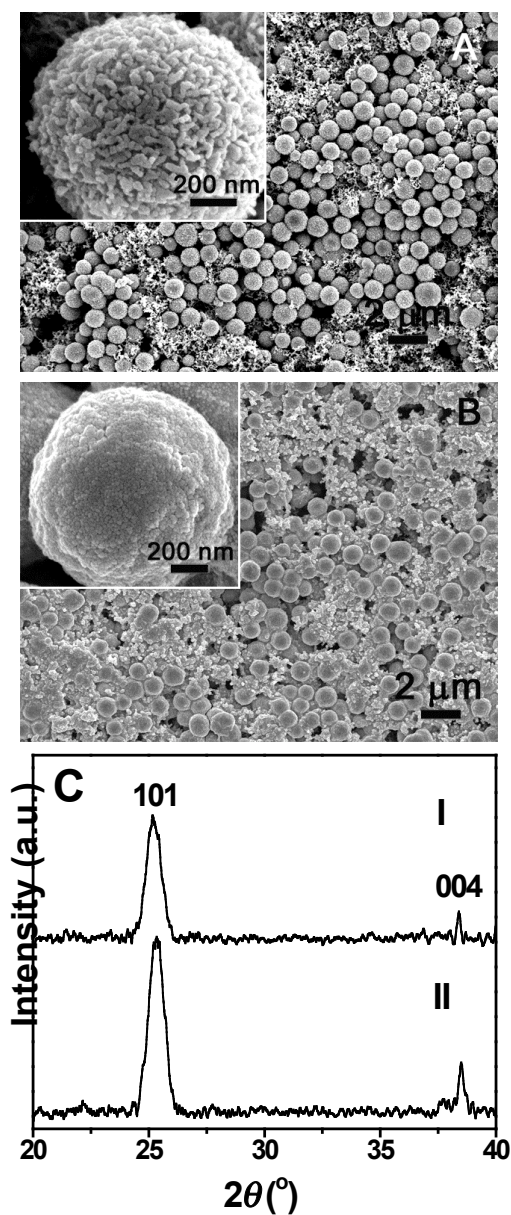
Figure 8. FESEM images of the anatase TiO_2-NSHS electrode before galvanostatic discharging/charging (A), and after 100 discharge-charge cycles at 5 C (850 mA g^{-1}) (B). The insets in (A) and (B) are the magnified FESEM images of the corresponding sample. (C) XRD patterns of the samples shown in (A) (I) and (B) (II).

TOC Graphic
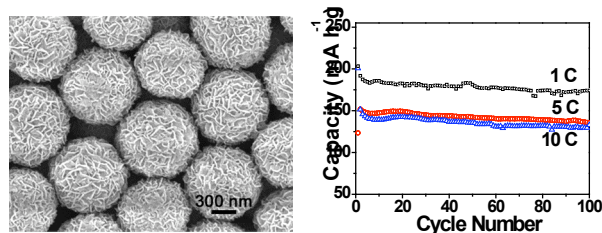
In this article, we report a facile synthesis of uniform hierarchical spheres self-assembled from large ultrathin anatase TiO_2 nanosheets with nearly 100% exposed (001) facets. We also show that the high surface density of exposed TiO_2 (001) facets and a well-defined nanoporous structure lead to fast lithium insertion/deinsertion processes in batteries that mimic features seen in high power electrochemical capacitors.